Can nuclear imaging accurately detect scar in ischemic CRT candidates?

Ganna Degtiarova, MD[1,2], Piet Claus, PhD[3], Jürgen Duchenne, PhD[3,4], Georg Schramm, PhD[1], Johan Nuyts, PhD[1], Jan Bogaert MD, PhD[5], Gabor Vöros, MD, PhD[3,4], Rik Willems, MD, PhD[3,4], Hein J. Verberne, MD, PhD[6], Jens-Uwe Voigt, MD, PhD[3,4], Olivier Gheysens MD, PhD[1,2,*]

1. Department of Imaging and Pathology, KU Leuven, Leuven, Belgium
2. Nuclear Medicine and Molecular Imaging, University Hospitals Leuven, Belgium
3. Department of Cardiovascular Sciences, KU Leuven, Leuven, Belgium
4. Department of Cardiovascular Diseases, University Hospitals Leuven, Leuven, Belgium
5. Department of Radiology, University Hospitals Leuven, Leuven, Belgium
6. Department of Radiology and Nuclear Medicine, Amsterdam UMC, location AMC, University of Amsterdam, The Netherlands

*current affiliation: Department of Nuclear Medicine, Cliniques Universitaires Saint-Luc, Brussel

E-mail addresses:
G.D.: gdegtiarova.work@gmail.com;
P.C.: piet.claus@kuleuven.be;
J.D.: jurgen.duchenne@kuleuven.be ;
G.S.: georg.schramm @kuleuven.be;
J.N.: johan.nuyts@kuleuven.be;
J.B.: jan.bogaert@uzleuven.be;
G.V.: gabor.voros@uzleuven.be;
R.W.: rik.willems@uzleuven.be;
H.J.V.: h.j.verberne@amsterdamumc.nl;
J-U.V.: jens-uwe.voigt@uzleuven.be;
O.G.: olivier.gheysens@uclouvain.be

Corresponding author:
Prof. Piet Claus
Cardiovascular Imaging and Dynamics
Department of Cardiovascular Sciences, KU Leuven,
Herestraat 49, box 7003 50,
3000 Leuven, Belgium
Tel.: +32/16/374653
Fax: +32/16/343467
E-mail: piet.claus@kuleuven.be

Submitting Author:
Ganna Degtiarova, MD, PhD
Department of Imaging and Pathology,
Nuclear Medicine & Molecular Imaging Unit,
UZ Herestraat 49 - box 7003, 3000 Leuven, Belgium
Email: gdegtiarova.work@gmail.com
Tel: +32 16 34 90 91

ABSTRACT (max 250 words)

Background: Accurate scar assessment is crucial in cardiac resynchronization therapy (CRT) candidates, since its presence is a negative predictor for CRT response. Therefore, we assessed the performance of different positron emission tomography (PET) parameters to detect scar in CRT candidates.

Methods: Twenty-nine CRT candidates underwent ^{18}F-FDG-PET/CT, resting ^{13}N-NH_3-PET/CT and cardiac magnetic resonance (CMR) prior to CRT implantation. Segmental ^{18}F-FDG uptake, late ^{13}N-NH_3 uptake and absolute myocardial blood flow (MBF) were evaluated for scar detection using late gadolinium enhancement (LGE) CMR as reference. A receiver operator characteristic (ROC)_ area under the curve (AUC) $\geq$ 0.8 indicated a good accuracy of the methods evaluated.

Results: Scar was present in 111 out of 464 segments. None of the approaches could reliably identify segments with non-transmural scar, except for ^{18}F-FDG uptake in the lateral wall (AUC 0.83). Segmental transmural scars could be detected with all methods (AUC $\geq$ 0.8), except for septal ^{18}F-FDG uptake and MBF in the inferior wall (AUC<0.8). Late ^{13}N-NH_3 uptake was the best parameter for transmural scar detection, independent of its location, with a sensitivity of 80% and specificity of 92% using a cut-off of 66% of the maximum tracer activity.

Conclusions: Late ^{13}N-NH_3 uptake is superior to ^{13}N-NH_3 MBF and ^{18}F-FDG in detecting transmural scar, independently of its location. However, none of the tested PET parameters was able to accurately detect non-transmural scar.

Key words: scar, cardiac resynchronization therapy, cardiac magnetic resonance, positron emission tomography.

INTRODUCTION

Cardiac resynchronization therapy (CRT) is a well-established treatment for patients with heart failure (HF) and broad QRS complex, however about 30% of patients do not respond to CRT [1]. Although no response to CRT is most likely a multifactorial issue, currently lacking a complete understanding, scar burden and scar distribution patterns have been reported as negative predictors for CRT outcome [2, 3]. Therefore, accurate detection of scar is essential to identify patients that are less likely to respond to CRT.

Late gadolinium enhancement (LGE) cardiac magnetic resonance (CMR) is currently the gold standard for assessing myocardial scar, however it cannot be performed in the presence of implantable devices/metallic implants and in patients with poor renal function or claustrophobia. Moreover, CMR requires a high level of expertise and CMR availability is sometimes an issue. Available alternative imaging modalities consist of echocardiography and nuclear imaging. Positron emission tomography (PET) with ^{13}N-NH_3 and ^{18}F-FDG to respectively assess perfusion and glucose metabolism, is a validated and clinically used technique to differentiate viable from non-viable myocardium. Viable myocardium is characterized by a preserved perfusion and metabolic activity or reduced perfusion with preserved metabolism (hibernation), while a concordant significant reduction in perfusion and metabolism is compatible with scar tissue.

This concept of detecting viable or scarred tissue with PET might be challenging in patients with ventricular conduction abnormalities. In previous work, we have demonstrated a heterogeneous regional distribution of absolute myocardial perfusion and glucose metabolism in non-ischemic CRT candidates [4, 5]. In particular, a low ^{13}N-NH_3-derived absolute myocardial blood flow (MBF) and ^{18}F-FDG uptake in the septum were observed with high values in the lateral wall, most likely representing a physiological adaptation of the heart to the alterations in myocardial workload and energy demands[6]. The redistribution of perfusion and metabolism, especially in the septum, may be challenging to reliably distinguish myocardial infarction from physiological changes in CRT candidates. We have previously demonstrated that, in contrast to ^{18}F-FDG uptake and ^{13}N-NH_3 MBF, late ^{13}N-NH3 uptake is relatively homogeneous across the heart in non-ischemic HF patients with ventricular conduction abnormalities, and might therefore be a more reliable parameter to detect scar in ischemic CRT candidates [5].

In the current study, we aimed to evaluate the performance of late ^{13}N-NH_3 uptake, ^{13}N-NH_3-derived MBF and ^{18}F-FDG uptake for scar detection and localization in ischemic CRT candidates, using LGE CMR as gold standard.

MATERIAL AND METHODS

Study Population

Patients referred for CRT implantation between August 2015 and November 2017 were prospectively recruited at the University Hospitals Leuven, Leuven, Belgium as part of the WORK-CRT study (ClinicalTrials.gov NCT02537782). Eligibility for CRT implantation was based on the 2013 ESC guidelines[7]. The main exclusion criteria were presence of right bundle branch block, recent myocardial infarction, valve surgery within 90 days prior to enrolment, history of heart transplantation or listed for heart transplantation, implanted LV assist device, severe aortic stenosis and uncorrected congenital heart disease. For this study, only patients who underwent ^{13}N-NH_3 PET, ^{18}F-FDG PET and CMR were analyzed.

Nuclear imaging

All patients underwent resting ^{13}N-NH_3 and gated ^{18}F-FDG PET studies (Biograph HiRez 16 PET/CT, Siemens, Erlangen, Germany) within 1 month before CRT implantation with a maximum 1 week time interval between both acquisitions. In case of a one-day protocol, ^{13}N-NH_3 always preceded ^{18}F-FDG scan with a minimum 60 minute interval between tracer administrations. A scout acquisition followed by a low-dose CT (80 kVp, 11 mAs) was performed before each PET emission for optimal patient positioning and subsequent CT-based attenuation correction. All static PET images were reconstructed using ordered-subsets expectation maximization algorithms (4 iterations and 8 subsets), matrix size 256 x 256 and a 5.0 mm Gaussian filter.

^{18}F-FDG PET/CT

All patients underwent a hyperinsulinemic euglycemic clamping technique to facilitate glucose consumption over fatty acid uptake, as previously described [8]. After reaching a steady state plasma glucose level, 4.25 MBq/kg ^{18}F-FDG was administered intravenously and a 40-minute ECG-gated acquisition was performed approximately 45 minutes after tracer administration.
ECG gated reconstruction (8 bins) of ^{18}F-FDG images was performed and the end-systolic bin was used for further analysis, based on previous results from our group [9]. ^{18}F-FDG scans were analyzed using in-house developed software [10]. Segmental ^{18}F-FDG uptake was evaluated according to the 17-segment American Heart Association model (excluding the apical segment 17) and expressed as percentage of the segment with the highest mean tracer uptake.

^{13}N-NH$_3$ PET/CT

A 30-minute dynamic list-mode acquisition was started together with an intravenous bolus administration of 740 MBq ^{13}N-NH$_3$. PET scans were analyzed both quantitatively and semi-quantitatively using in-house developed software [10]. For segmental absolute MBF quantification, the list-mode file was rebinned into 22 frames (12 frames x 10 sec, 4 frames x 30 sec, 3 frames x 120 sec, 1 frame x 180 sec, 1 frame 420 sec, and 1 frame x 600 sec) and a two-tissue compartment model was applied on the first 10 minutes of the acquisition [11]. Estimated rate constants were calculated using a weighted least-square method and were corrected for partial volume effect, spillover and metabolites as previously reported [10, 12]. Segmental late ^{13}N-NH$_3$ uptake was derived from a static reconstructed image (20-30 min) and values were expressed as percentage of the segment with the highest mean tracer uptake.

CMR and scar analysis

CMR was performed within 1 month before CRT implantation using a 1.5 Tesla Ingenia (Philips Healthcare, Best, the Netherlands). LGE images were acquired during steady state after intravenous injection of 0.15 mmol/kg gadoterate meglumine (Doteram™, Guerbet, Villepinte, France). CMR analysis was done visually and by consensus of two experienced radiologists, blinded to clinical data and PET results. Segmental scar analysis was performed using the 17-segment model. using a standardized segmentation scheme, which allows to compare segments across imaging modalities[13]. Briefly, the LV was divided into three equal parts, with papillary muscles serving as a reference for midwall. Right ventricle insertion points were used to differentiate septum from anterior and inferior wall, with lateral wall being opposite to the septum. Segment 17 (apex) was excluded from the analysis. Each of the 16 segments was assigned a score based on the presence and extent of LGE using the following scale: 0 – no hyperenhancement, 0.5 – hyperenhancement ≤ 50% of the segmental volume and 1 – hyperenhancement > 50% of the segmental volume[14, 15]. Segments with a score of 1 were considered to have a transmural scar.

Statistical Analysis

Statistical analysis was performed using MedCalc ® v.10.3.0 software. Normally distributed continuous variables were expressed as mean ± standard deviation while categorical variables were represented as percentages. A 2 way ANOVA with post hoc correction was used to compare MBF, late ^{13}N-NH^3 uptake and ^{18}F-FDG uptake within segments. The ability of each

nuclear imaging parameter to detect segmental scar was tested using receiver operating characteristic curve (ROC) with segmental CMR LGE score serving as reference. An area under the curve (AUC) ≥ 0.80 indicated a good diagnostic performance (i.e., accuracy) of parameters evaluated. In case of good agreement, an optimal PET cut-off value was determined to detect transmural or non-transmural scar. A p-value of less than 0.05 was considered statistically significant.

RESULTS

Patient characteristics

Twenty-nine patients were included and patient characteristics are summarized in Table 1.

LGE-CMR results for segmental scar assessment

Among 464 analyzed segments, 36 (8%) segments had transmural scar, 75 (16%) segments had non-transmural scar, while 353 (76%) segments did not have any evidence of scar on LGE CMR scans. Table 2 provides a detailed regional distribution of segments with and without scar.

PET results for segmental scar assessment

Table 3 summarizes the mean segmental values for absolute MBF, late ^{13}N-NH_3 uptake and ^{18}F-FDG uptake in scarred and non-scarred tissue in each myocardial wall.

Segments without scar

Absolute MBF and ^{18}F-FDG uptake showed regional heterogeneity with lowest values in the septum and highest in the lateral wall, while late ^{13}N-NH_3 was rather homogenously distributed.

Non-transmural scar

The average segmental MBF and ^{18}F-FDG uptake in segments with non-transmural scar was significantly lower in the septum compared to the other walls, except for MBF in the inferior wall. Late ^{13}N-NH_3 segmental uptake showed a homogeneous distribution.

Segmental ^{18}F-FDG uptake in the lateral wall was the only parameter that demonstrated a good agreement with CMR LGE (AUC>0.8), with a cut-off value ≤ 77% yielding a sensitivity and specificity of 80% and 84% respectively (Figure 1A-D).

Transmural scar

Segmental ^{18}F-FDG uptake and MBF were significantly higher in the lateral wall compared to all other regions (ANOVA F=3.2, p=0.03). Late ^{13}N-NH_3 segmental uptake was equally decreased across the myocardial walls.

Septal segments

Absolute MBF and late ^{13}N-NH$_3$ uptake demonstrated a good agreement with LGE CMR for the detection of segments with transmural scar (AUC 0.84 [0.76-0.89] and AUC 0.91 [0.86-0.95], respectively, both p<0.0001), while a poor agreement was observed for ^{18}F-FDG uptake (AUC<0.8, p=0.005). The optimal cut-off values for ^{13}N-NH$_3$ MBF and late ^{13}N-NH$_3$ were 0.4 ml/g/min and 65% which resulted in a sensitivity and specificity of 64% and 89%, and 82% and 96%, respectively (Figure 2A).

Lateral wall segments

All three approaches demonstrated a good agreement with LGE CMR (AUC>0.8, p<0.0001). Segmental ^{18}F-FDG uptake ≤ 76 % could detect transmural scar with a sensitivity of 88% and specificity of 79%, while a cut-off of ≤ 0.65 ml/g/min for MBF and ≤ 62 % for late ^{13}N-NH$_3$ resulted in a sensitivity and specificity of respectively 75%, 75% and 75%, 96% (Figure 2B).

Anterior wall segments

Similar to the lateral wall, all PET parameters demonstrated a good agreement with LGE CMR (AUC>0.8, p<0.0001) (Figure 3A).

Inferior wall segments

^{18}F-FDG uptake and late ^{13}N-NH$_3$ uptake demonstrated a good agreement with LGE CMR (AUC>0.8, p<0.0001), while ^{13}N-NH$_3$ MBF did not show a good agreement (AUC<0.8, <0.0001). The sensitivity and specificity of segmental ^{18}F-FDG uptake ≤ 45% were 100% and 77%, respectively, while a cut-off of ≤ 63% for late ^{13}N-NH$_3$ uptake these yielded a sensitivity and specificity of 73% and 89% respectively (Figure 3B).

All myocardial segments

Late ^{13}N-NH$_3$ uptake was the only parameter that could reliably detect segmental transmural scar independently of the myocardial region (Figure 4). Further analysis revealed that a cut-off value of ≤ 66% could detect the presence of transmural scar with a sensitivity of 80% and specificity of 92%, independently of myocardial territory (Figure 5).

DISCUSSION

The main finding of the present study is that semiquantitative segmental late ^{13}N-NH_3 uptake is superior to ^{13}N-NH_3-derived MBF and ^{18}F-FDG uptake to detect transmural myocardial scar in CRT candidates, independently of its location.

In the current study, we evaluated the performance of ^{18}F-FDG uptake, absolute ^{13}N-NH_3-derived MBF and late ^{13}N-NH_3 uptake to detect myocardial scar in CRT eligible patients with a history of ischemic heart disease. None of the PET derived parameters, except for ^{18}F-FDG uptake in the lateral wall, could reliably detect segments with non-transmural scar. Several factors, such as limited spatial resolution and the resulting partial volume effect, could contribute to the low performance of nuclear imaging techniques to detect subendocardial scars [16, 17]. In our study, ^{18}F-FDG uptake was calculated using the end-systolic gate. The end-systolic frame in CRT candidates is mainly associated with a contraction of the lateral wall, which has a larger amplitude and relates to the higher regional workload[6]. Thus, during this end-systolic phase, the lateral wall is the most thickened region, hereby suffering less from partial volume effects. This may at least partially explain the high AUC of gated ^{18}F-FDG PET to detect non-transmural scar in the lateral wall.

In contrast to non-transmural scars and in line with the literature, a good agreement was observed between different PET derived parameters and CMR for the detection of transmural scars [17]. However, in contrast to other published studies evaluating the performance of PET in a general ischemic population, in CRT eligible patients a considerable variation of the performance of each PET parameter was observed between LV walls. For example in the septum, ^{13}N-NH_3 MBF and late ^{13}N-NH_3 uptake showed to have a good diagnostic accuracy using CMR as a reference to detect transmural scar, but poor diagnostic accuracy was observed for ^{18}F-FDG PET. Previously, several groups have shown that non-ischemic CRT candidates demonstrated a physiologically low septal glucose metabolism and myocardial perfusion, reflecting the adaptation of the heart to the differential regional myocardial workload [18, 19]. In the current study, we also observed the presence of low average ^{18}F-FDG uptake and ^{13}N-NH_3 MBF in septal segments without scar. However, a large overlap in ^{18}F-FDG uptake was observed between transmurally scarred and normal septal segments (32±11% vs 42±14% respectively), explaining the low AUC for ^{18}F-FDG uptake. In contrast to metabolic activity, septal MBF showed a good overall performance to detect transmural scar, but the cut-off of 0.4 ml/g/min yielded a relatively low sensitivity. In contrast to ^{18}F-FDG and absolute MBF, late ^{13}N-NH_3 uptake could detect septal segments with transmural scar with high diagnostic

accuracy. This is in line with our previous results in non-ischemic CRT candidates demonstrating that late ^{13}N-NH_3 uptake does not mirror regional distribution of ^{13}N-NH_3 MBF, but has a rather homogenous distribution across the heart[5]. Immediately after crossing the cardiomyocyte membrane, ^{13}N-NH_3 is metabolized suggesting that late ^{13}N-NH_3 uptake is an indirect maker of metabolic integrity and cell viability[20]. Therefore, a decrease in late ^{13}N-NH_3 uptake can be mainly attributed to the presence of myocardial scar. The latter is supported by a pronounced difference and lack of overlap between the average ^{13}N-NH_3 uptake in the healthy and infarcted septal segments (80±9% vs 57±11%).

In the lateral wall, all nuclear parameters could reliably detect the presence of transmural scar. Interestingly, the optimal cut-off value for MBF determined in this study to detect transmural scar in the lateral wall (0.65 ml/g/min) was higher than for the septal wall (0.4 ml/g/min) and higher than reported values for the general population (0.45 ml/g/min) [21, 22]. Similar to MBF, a higher cut-off value for ^{18}F-FDG uptake (76%) to detect transmural scar in the lateral segments was obtained in our study, compared to the widely used 50% cut-off to define transmural scar [23]. These differences in cut-off values can be explained by the definition of transmural scar, used in our study. Segments with transmural scar encompassed those with a hyperenhancement ranging between 50 and 100% of the segmental volume, meaning that part of the segment could still consist of viable tissue. In addition, the higher perfusion and glucose uptake in the lateral wall of a CRT-eligible heart, is another mechanism that could contribute to the higher cut-off values for ^{18}F-FDG and MBF for transmural scar detection[5].

As discussed earlier, ^{18}F-FDG and ^{13}N-NH_3 do not solely reflect metabolism, perfusion and their relation, but both tracers are affected by the disease itself and reflect underlying pathophysiological adaptations of the myocardium. These adaptations in CRT eligible patients are most obvious in septal and lateral segments. The matter might explain that all PET approaches could equally well define the presence of segments with transmural scar in the anterior and inferior wall, except for MBF in the inferior wall. Even though no firm explanation is available, one hypothesis could be the higher susceptibility of MBF in the inferior wall to noise and interference with neighboring organs (e.g. liver). Amongst all parameters, late ^{13}N-NH_3 uptake showed an overall good agreement with LGE CMR to define segments with transmural scar independently of myocardial region. In addition, a single late ^{13}N-NH_3 uptake cut-off of ≤66% provided a good with LGE CMR and was able to accurately detect transmural scar with high sensitivity and specificity in ischemic CRT candidates.

STUDY LIMITATIONS

In this study, only visual assessment of LGE CMR was performed to detect scar. However, previous studies have shown that visual analysis of CMR scans correlates good with automated quantification of scar extent [24].

It would be interesting to explore in a larger cohort of patients the influence of subendocardial/non-transmural scars on CRT response and outcome since we have shown that PET underestimates the presence and extent of these scars. The latter will provide important information with regard to the possible use of PET as a reliable alternative to CMR for the management of patients with ventricular conduction delays.

CONCLUSIONS

Late ^{13}N-NH_3 uptake is superior to ^{13}N-NH_3 MBF and ^{18}F-FDG uptake to detect the presence of transmural scar, independently of its location, in ischemic CRT eligible patients. In contrast to a general population, the ability of ^{18}F-FDG uptake and ^{13}N-NH_3 MBF to detect transmural scar in CRT candidates varies considerably across LV walls, with the septum being the most challenging region. None of the PET parameters is suited to accurately detect non-transmural scars in this CRT eligible cohort.

Funding: This work was supported by a KU Leuven research grant [OT/12/084].

Conflicts of interest: RW reports research funding from Biotronik, Boston Scientific, Medtronic; speakers and consultancy fees from Medtronic, Boston Scientific, Biotronik, Abbott, Microport. RW is supported as postdoctoral clinical researcher by the Fund for Scientific Research Flanders. All other authors report no relationships that could be construed as a conflict of interest.

Ethics approval and consent to participate: The study was approved by the local institutional ethics committee and all patients gave written and informed consent prior to inclusion. The WORK-CRT study was registered at ClinicalTrials.gov (NCT02537782).

Consent for publication: Consent for publication has been obtained from the patients.

Availability of data and material: The datasets used and/or analysed during the current study are available from the corresponding author on reasonable request.

REFERENCES

1. Ypenburg C, Westenberg JJ, Bleeker GB, et al (2008) Noninvasive Imaging in Cardiac Resynchronization Therapy-Part 1: Selection of Patients. Pace-Pacing Clin Electrophysiol 31:1475–1499. https://doi.org/10.1111/j.1540-8159.2008.01212.x

2. Mangiavacchi M, Gasparini M, Faletra F, et al (2006) Clinical predictors of marked improvement in left ventricular performance after cardiac resynchronization therapy in patients with chronic heart failure. Am Heart J 151:477.e1-477.e6. https://doi.org/10.1016/j.ahj.2005.08.008

3. Chung ES, Leon AR, Tavazzi L, et al (2008) Results of the Predictors of Response to CRT (PROSPECT) trial. Circulation 117:2608–16. https://doi.org/10.1161/CIRCULATIONAHA.107.743120

4. Degtiarova G, Claus P, Duchenne J, et al (2019) Low septal to lateral wall 18F-FDG ratio is highly associated with mechanical dyssynchrony in non-ischemic CRT candidates. EJNMMI Res 9:105. https://doi.org/10.1186/s13550-019-0575-9

5. Degtiarova G, Claus P, Duchenne J, et al (2019) Impact of left bundle branch block on myocardial perfusion and metabolism: A positron emission tomography study. J Nucl Cardiol. https://doi.org/10.1007/s12350-019-01900-y

6. Duchenne J, Turco A, Ünlü S, et al (2019) Left Ventricular Remodeling Results in Homogenization of Myocardial Work Distribution. Circ Arrhythmia Electrophysiol 12:1–14. https://doi.org/10.1161/CIRCEP.118.007224

7. Brignole M, Auricchio A, Baron-Esquivias G, et al (2013) 2013 ESC Guidelines on cardiac pacing and cardiac resynchronization therapy: The Task Force on cardiac pacing and resynchronization therapy of the European Society of Cardiology (ESC). Developed in collaboration with the European Heart Rhythm Association (EHRA). Europace 15:1070–1118. https://doi.org/10.1093/europace/eut206

8. Lewis P, Nunan T, Dynes A, Maisey M (1996) The use of low-dose intravenous insulin in clinical myocardial F-18 FDG PET scanning. Clin Nucl Med 21:15–8

9. Turco A, Gheysens O, Duchenne J, et al (2019) Partial volume and motion correction in cardiac PET: First results from an in vs ex vivo comparison using animal datasets. J Nucl Cardiol. https://doi.org/10.1007/s12350-018-01581-z

10. Nuyts J, Suetens P, Oosterlinck A, et al (1991) Delineation of ECT images using global constraints and dynamic programming. IEEE Trans Med Imaging 10:489–98. https://doi.org/10.1109/42.108582

11. Hutchins GD, Schwaiger M, Rosenspire KC, et al (1990) Noninvasive quantification of regional blood flow in the human heart using N-13 ammonia and dynamic positron emission tomographic imaging. J Am Coll Cardiol 15:1032–42

12. Bormans G, Maes A, Langendries W, et al (1995) Nuclear Medicine Original article Metabolism of nitrogen-13 labelled ammonia in different. 22:

13. Cerqueira MD, Weissman NJ, Dilsizian V, et al (2002) Standardized Myocardial Segmentation and Nomenclature for Tomographic Imaging of the Heart. Circulation 105:539–542. https://doi.org/10.1161/hc0402.102975

14. Palazzuoli A, Beltrami M, Gennari L, et al (2015) The impact of infarct size on regional and global left ventricular systolic function: a cardiac magnetic resonance imaging study. Int J Cardiovasc Imaging 31:1037–44. https://doi.org/10.1007/s10554-015-0657-3

15. Gaibazzi N, Bianconcini M, Marziliano N, et al (2016) Scar Detection by Pulse-Cancellation Echocardiography. JACC Cardiovasc Imaging 9:1239–1251. https://doi.org/10.1016/j.jcmg.2016.01.021

16. Roes SD, Kaandorp TAM, Marsan NA, et al (2009) Agreement and disagreement between contrast-enhanced magnetic resonance imaging and nuclear imaging for assessment of myocardial viability. Eur J Nucl Med Mol Imaging 36:594–601. https://doi.org/10.1007/s00259-008-1001-0

17. Klein C, Nekolla SG, Bengel FM, et al (2002) Assessment of myocardial viability with contrast-enhanced magnetic resonance imaging: comparison with positron emission tomography. Circulation 105:162–7. https://doi.org/10.1161/hc0202.102123

18. Baller D, Vogt J, Lindner O, et al (2004) Myocardial oxygen consumption and perfusion before and after cardiac resynchronization therapy: Experimental observations and clinical implications. Eur Hear Journal, Suppl 6:. https://doi.org/10.1016/j.ehjsup.2004.05.001

19. Nowak B, Sinha AM, Schaefer WM, et al (2003) Cardiac resynchronization therapy

homogenizes myocardial glucose metabolism and perfusion in dilated cardiomyopathy and left bundle branch block. J Am Coll Cardiol 41:1523–1528. https://doi.org/10.1016/S0735-1097(03)00257-2

20. Kitsiou AN, Bacharach SL, Bartlett ML, et al (1999) 13N-ammonia myocardial blood flow and uptake: relation to functional outcome of asynergic regions after revascularization. J Am Coll Cardiol 33:678–86

21. Beanlands RS, DeKemp R, Scheffel A, et al (1997) Can nitrogen-13 ammonia kinetic modeling define myocardial viability independent of fluorine-18 fluorodeoxyglucose? J Am Coll Cardiol 29:537–43

22. Benz DC, Ferro P, Safa N, et al (2019) Role of quantitative myocardial blood flow and 13N-ammonia washout for viability assessment in ischemic cardiomyopathy. J Nucl Cardiol. https://doi.org/10.1007/s12350-019-01684-1

23. Knuesel PR, Nanz D, Wyss C, et al (2003) Characterization of dysfunctional myocardium by positron emission tomography and magnetic resonance: relation to functional outcome after revascularization. Circulation 108:1095–100. https://doi.org/10.1161/01.CIR.0000085993.93936.BA

24. Schuijf JD, Kaandorp TAM, Lamb HJ, et al (2004) Quantification of myocardial infarct size and transmurality by contrast-enhanced magnetic resonance imaging in men. Am J Cardiol 94:284–8. https://doi.org/10.1016/j.amjcard.2004.04.020

Figures

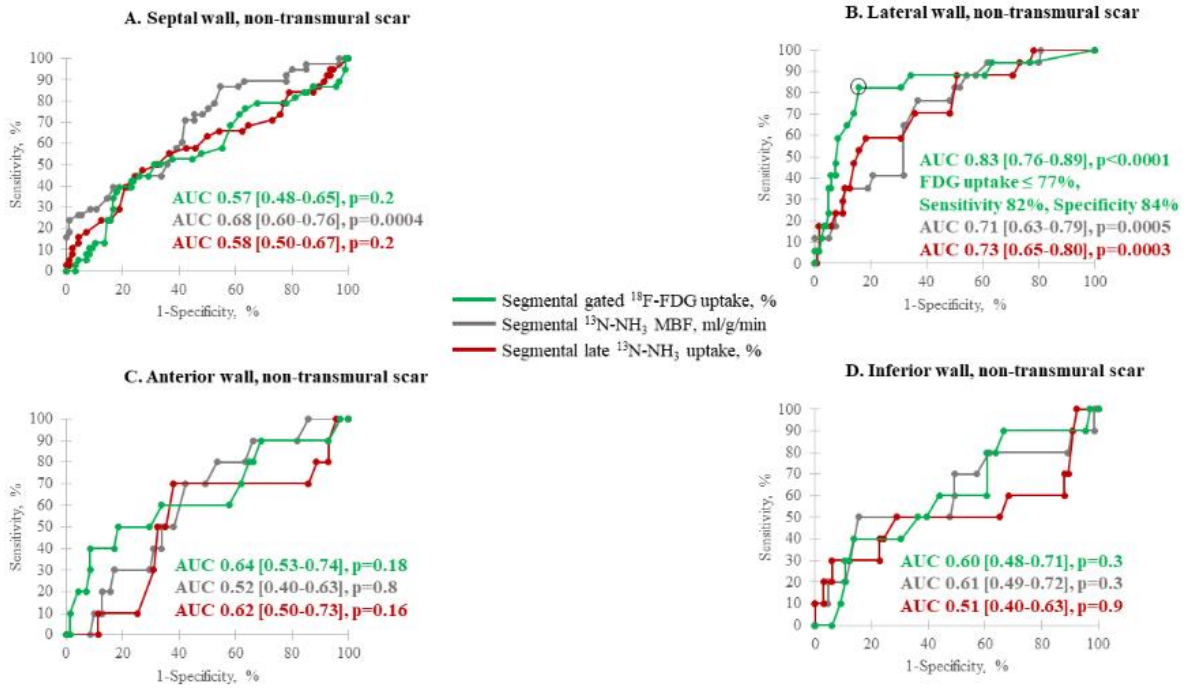

Figure 1. ROC curves for different nuclear imaging approaches to detect the presence of segmental non-transmural scar in the septal (A), lateral (B), anterior (C) and inferior (D) wall.

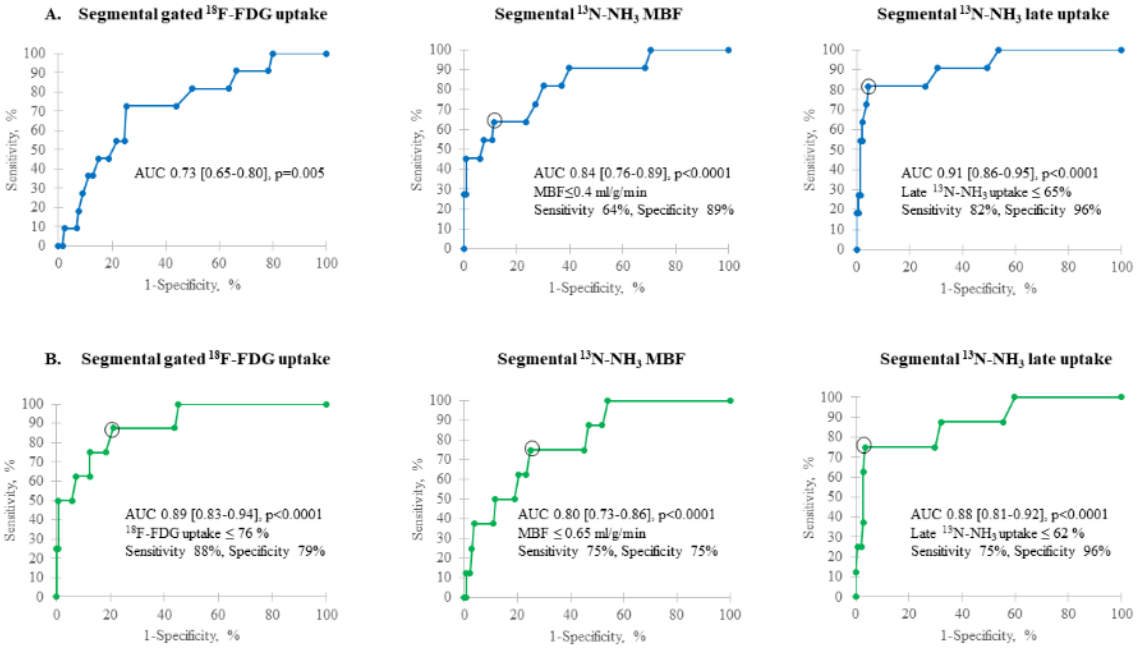

Figure 2. ROC curves for different nuclear imaging approaches to detect the presence of segmental transmural scar in the septal (A) and lateral (B) wall

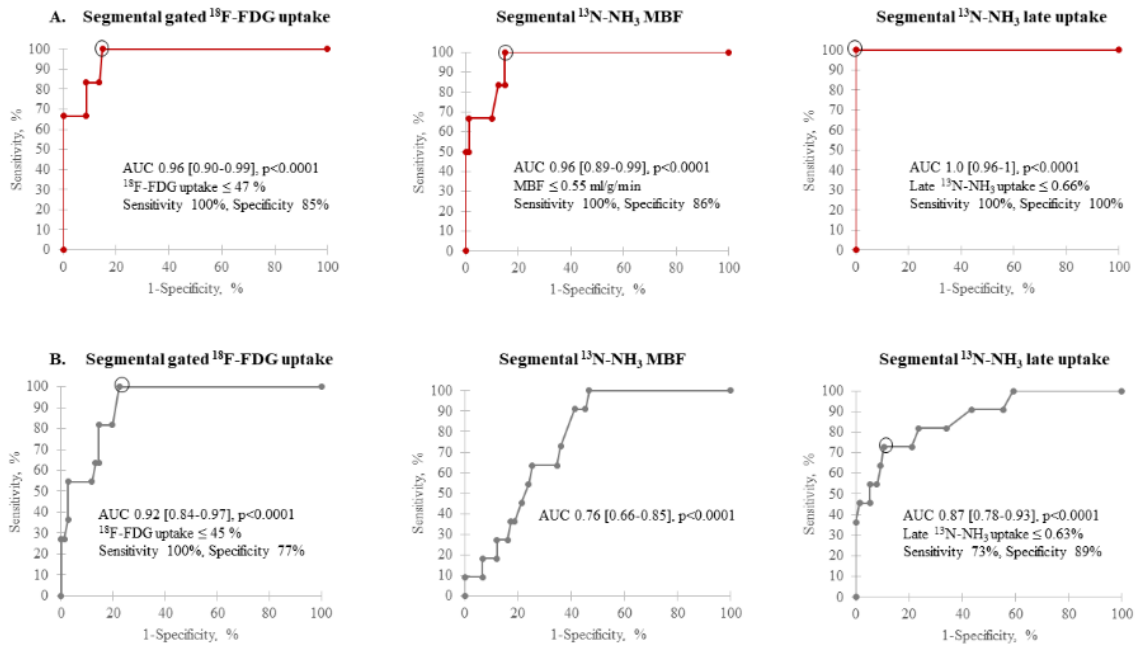

Figure 3. ROC curves for different nuclear imaging approaches to detect the presence of segmental transmural scar in the anterior (A) and inferior (B) wall

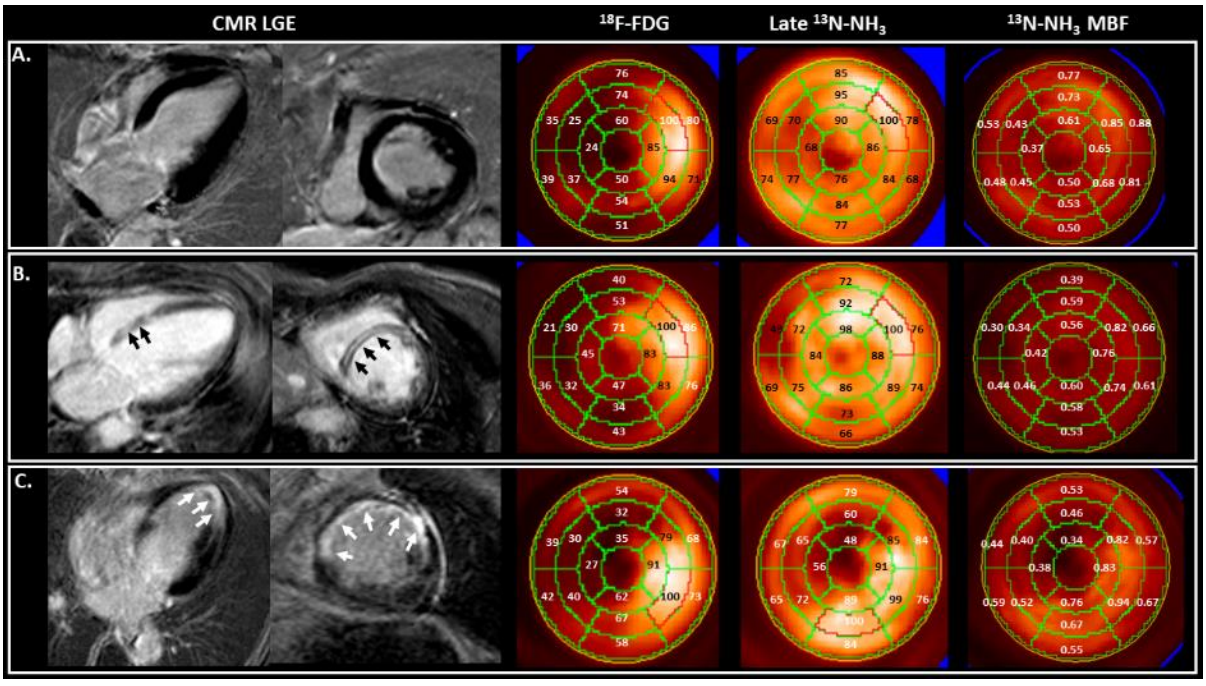

Figure 4. Representative examples of ^{18}F-FDG, late ^{13}N-NH$_3$ and ^{13}N-NH$_3$ -derived absolute MBF polar maps in LBBB patients without myocardial scar (A), with non-transmural myocardial scar (B) and with transmural myocardial scar (C) on late-gadolinium enhancement CMR. Values on the ^{18}F-FDG and late ^{13}N-NH$_3$ polar maps are represented as percentage of the segment with the highest mean tracer uptake. Values on ^{13}N-NH$_3$ MBF polar map are expressed as ml/min/g tissue.

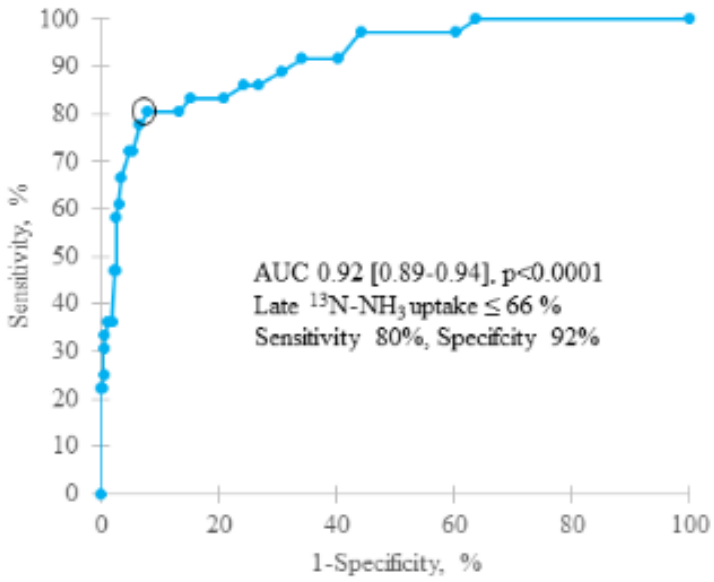

Figure 5. ROC curve for late ^{13}N-NH$_3$ uptake to detect the presence of segmental transmural scar, independently of its location.

Table 1. Clinical patient characteristics

Parameter	All patients (n=29)
Male (%)	17 (59%)
Age (y)	68±8
Diabetes mellitus (%)	3 (10%)
Blood pressure (mmHg)	133±20 / 71±15
Left ventricular function:	
EDV (ml)	161±58
ESV (ml)	111±48
EF (%)	33±9
NYHA class:	
NYHA 2	18(62%)
NYHA 3	11(38%)
QRS width (ms)	160±20
Medication:	
β-blockers	25(86%)
ACEi/ARB	27(93%)
Aldosterone antagonists	17(59%)

ACEi - angiotensin converting enzyme inhibitors; ARB - angiotensin-receptor blockers; EDV – end-diastolic volume; ESV – end-systolic volume, EF - ejection fraction.

Table 2. Distribution of segments with and without scar defined by visual assessment of LGE CMR

	No scar	Non-transmural scar	Transmural scar
Septal wall Segments, N	96	38	11
Lateralwall segments, N	120	17	8
Anterior wall segments, N	71	10	6
Inferior wall segments, N	66	10	11

Table 3. Myocardial blood flow, late ^{13}N-NH_3 uptake and ^{18}F-FDG uptake in segments with and without scar, represented per myocardial region

	^{13}N-NH_3 MBF, ml/g/min	Late ^{13}N-NH_3 uptake, %	^{18}F-FDG uptake, %
Septal segments			
No scar	0.59±0.17*$	80±9	42±14#&
Non-transmural scar	0.50±0.13	78±12	45±15
Transmural scar	0.41±0.13	58±11*	32±11
Lateral wall segments			
No scar	0.85±0.26*&	83±12*	88±11*&
Non-transmural scar	0.67±0.19	74±11	74±12*
Transmural scar	0.57±0.18	62±13	61±16*
Anterior wall segments			
No scar	0.7±0.14	88±8&	60±14&
Non-transmural scar	0.69±0.11	88±10	69±19
Transmural scar	0.42±0.08*	57±8*	34±8*
Inferior wall segments			
No scar	0.66±0.14	78±10	54±12&
Non-transmural scar	0.71±0.20	75±14	52±11
Transmural scar	0.54±0.12*	56±16*	34±9*

*$p<0.05$ compared to the other scar type within the same wall

# $p<0.05$ compared to transmural scar

& $p<0.05$ compared to segments without scar in all other heart regions

$ $p<0.05$ compared to segments without scar in theanterior wall